Impact of Hydrodynamic Interactions on the Kinetic Pathway of Protein Folding

Jiaxing Yuan[1] and Hajime Tanaka[1,2,*]

[1]Research Center for Advanced Science and Technology, The University of Tokyo, 4-6-1 Komaba, Meguro-ku, Tokyo 153-8904, Japan
[2]Department of Fundamental Engineering, Institute of Industrial Science, The University of Tokyo, 4-6-1 Komaba, Meguro-ku, Tokyo 153-8505, Japan

(Received 21 March 2023; accepted 29 February 2024; published 27 March 2024)

Protein folding is a fundamental process critical to cellular function and human health, but it remains a grand challenge in biophysics. Hydrodynamic interaction (HI) plays a vital role in the self-organization of soft and biological materials, yet its role in protein folding is not fully understood despite folding occurring in a fluid environment. Here, we use the fluid particle dynamics method to investigate many-body hydrodynamic couplings between amino acid residues and fluid motion in the folding kinetics of a coarse-grained four-α-helices bundle protein. Our results reveal that HI helps select fast folding pathways to the native state without being kinetically trapped, significantly speeding up the folding kinetics compared to its absence. First, the directional flow along the protein backbone expedites protein collapse. Then, the incompressibility-induced squeezing flow effects retard the accumulation of non-native hydrophobic contacts, thus preventing the protein from being trapped in local energy minima during the conformational search of the native structure. We also find that the significance of HI in folding kinetics depends on temperature, with a pronounced effect under biologically relevant conditions. Our findings suggest that HI, particularly the short-range squeezing effect, may be crucial in avoiding protein misfolding.

DOI: 10.1103/PhysRevLett.132.138402

Protein folding is vital for achieving a functional three-dimensional structure, known as a native state, through amino acid interactions [1]. Recent advancements in artificial intelligence have enabled accurate prediction of native structures from amino acid sequences [2,3]. However, understanding nonequilibrium folding pathways to access these native structures remains a grand challenge [4–10], as proteins often encounter kinetic barriers before reaching their global free-energy minimum state [8], leading to metastable intermediates.

Hydrodynamic interaction (HI) induced by solvent flow could significantly affect protein folding by dynamically coupling the motion of amino acid residues, yet this aspect has been less explored [11,12]. Most coarse-grained simulations of protein folding have adopted Langevin dynamics and Brownian dynamics (BD), both of which neglect HI between amino acid residues through solvent [13–24]. For a polymer in a solvent, HI was shown to accelerate the collapsing [25–27]. The effects of HI on the folding of α helix and β hairpin were explored by pioneering simulations but reported negligible [26,28]. Subsequent simulation studies revealed that HI accelerates folding by 2–3 times for specific proteins [29,30]. A recent work also reported that HI can either speed up or slow down folding kinetics depending on the temperature [31]. These prior studies provide valuable insights into the roles of HI [26,28–31]: HI tends to speed up the protein collapsing [12], as observed in the coil-globule transition of homopolymers [25,26,32–34]. However, HI appears to have a minor impact on the selection of folding pathways [12,29].

To our knowledge, previous simulations [26,28–31] have frequently employed Rotne-Prager tensor for modeling HI [35,36]. However, we note that Rotne-Prager tensor [35] cannot properly account for the short-range many-body HI arising from the fluid incompressibility that tends to prevent particles from closely approaching each other to form densely packed arrangements. This short-range contribution, known as "squeezing flow effect" [11,33,37,38] (also called "lubrication effect" [39–43]; we use the term "squeezing flow" throughout this Letter), is essential for modeling phase ordering kinetics of soft materials [37,38,44–47]. Therefore, in situations where the incompressibility condition must be satisfied, the most suitable simulation method is directly solving the Navier-Stokes (NS) equation.

In this Letter, we employ the fluid particle dynamics (FPD) method [33,48,49] based on the direct computation of the NS equation to study the folding kinetics of four-α-helices bundle protein [17]. We find that HI facilitates the selection of fast folding pathways, leading to rapid attainment of the native state without kinetic trapping, and significantly accelerates folding kinetics compared to their absence. Specifically, directional flow speeds up collapsing during protein folding, consistent with previous findings [12]. Notably, the incompressibility-induced squeezing flow [33] plays a crucial role in establishing proper hydrophobic contacts by preventing the accumulation of non-native interactions and avoiding trapping the protein in local energy minima, which is crucial for selecting fast folding pathways.

 © 2024 American Physical Society

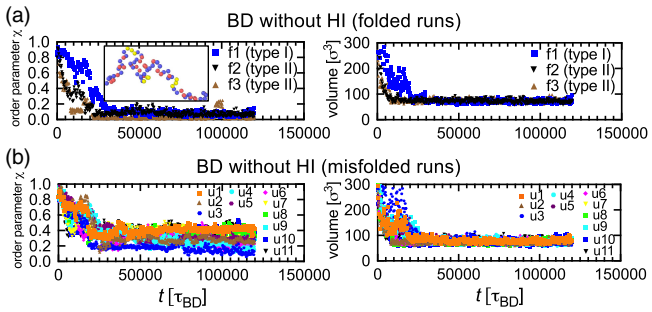

FIG. 1. Folding kinetics of four-α-helices bundle protein in the absence of HI. Temporal change of order parameter χ and protein volume for (a) folded and (b) misfolded trajectories in BD simulations (at $k_BT/\varepsilon = 0.6$). The inset of (a) shows a typical initial configuration of a swollen amino acid coil at $k_BT_{\rm init}/\varepsilon = 1$. The protein volume is determined by calculating the convex hull [51] of amino acid residues.

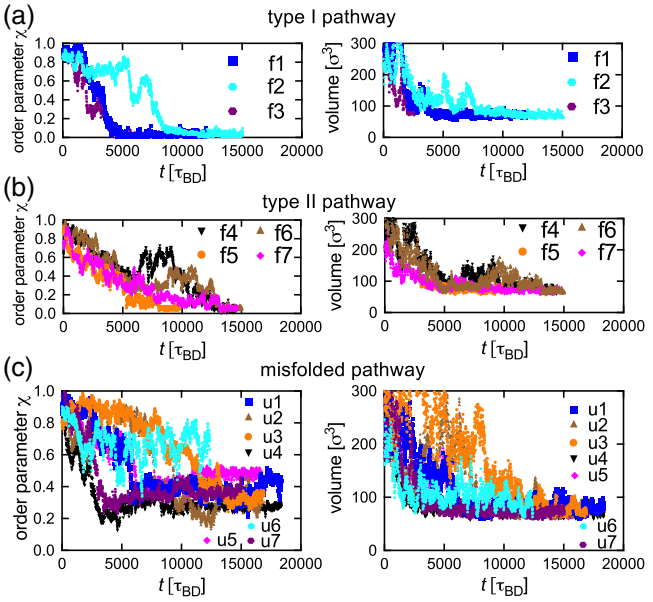

FIG. 2. Folding kinetics of four-α-helices bundle protein in the presence of HI. Temporal change of order parameter χ and protein volume for (a),(b) folded and (c) misfolded trajectories in FPD simulations (at $k_BT/\varepsilon = 0.6$). The presence of HI promotes the selection of type I and type II folding pathways and significantly reduces the folding time. We classify folding pathways into two types based on the chronological order of collapse and folding. See text for details.

We simulate a four-α-helices bundle protein [17] placed in a cubic three-dimensional periodic box using the FPD method [33,48,49] (Appendix A). The folding temperature T_f is $k_BT_f/\varepsilon \simeq 0.7$, where k_B is the Boltzmann constant and ε is the energy coupling of Lennard-Jones potential [17] (see Supplemental Material [50]). Figure 5 in Appendix A shows the native structure obtained by slowly cooling the system to zero temperature. We prepare the initial configuration [see, e.g., the inset of Fig. 1(a)] at $k_BT_{\rm init}/\varepsilon = 1$, and then, instantaneously quench the system to $T < T_f$. Time is measured in units of the Brownian time for a single free bead, τ_{BD}. We focus on the quench depth of $k_BT/\varepsilon = 0.6$. However, we demonstrate that our findings also hold for $k_BT/\varepsilon = 0.65$. To characterize the folding kinetics, we adopt the structure order parameter χ [16,17].

As a reference system, we first explore the folding kinetics using BD simulations without HI (Fig. 1). We find that only 3 out of 14 trajectories reach the correct folded state, characterized by $\chi \approx 0$ (see Ref. [50] for the definition of χ), before $t \approx 1.2 \times 10^5 \tau_{BD}$ [Fig. 1(a)]. We classify these successful folding pathways into two types, depending on the chronological order of folding [Fig. 1(a), left] and collapse [Fig. 1(a), right]: the collapse and folding occur almost concurrently for the type I pathway [$f1$ in Fig. 1(a)], whereas in the type II pathway [$f2 - f3$ in Fig. 1(a)], folding is completed significantly later than the collapse. In the majority of instances, proteins are trapped in misfolded intermediates with $\chi \approx 0.2$–0.4 [Fig. 1(b), left] despite being collapsed [Fig. 1(b), right]. Among all the simulations we conducted, the quickest folding pathway has a folding time of approximately $t_f \approx 2 \times 10^4 \tau_{BD}$. Even though the native structure of the four-α-helices bundle protein seems simple, misfolded pathways are quite often selected [Fig. 1(b)].

The situation becomes far more different when HI is included (Fig. 2). Seven out of 14 trajectories reach the correct folded state [Figs. 2(a) and 2(b)] within a much shorter time $t_f = 5 \times 10^3 \tau_{BD} - 1.5 \times 10^4 \tau_{BD}$. In the remaining simulations, proteins remain misfolded until the end of the simulation [Fig. 2(c)]. Note, however, that due to the computational constraints, the accessible simulation time for FPD is approximately 7 to 8 times shorter than with BD, reflecting higher computational costs associated with FPD due to the need to calculate the flow field at each time step using NS equation. Thus, some of the misfolded states in Fig. 2(c) might eventually fold if the FPD simulation covers the same amount of time as BD. The shortest folding time among these fast folding pathways [$f1$ and $f3$ in Fig. 2(a)] is $t_f \approx 5000 \tau_{BD}$. These results indicate that HI promotes the selection of type I and type II folding pathways and reduces the likelihood of misfolded pathways (Fig. 2), compared to BD simulations without HI (Fig. 1). Additional trajectories from FPD simulations in the Supplemental Material (Fig. S1 in [50]) further support our findings. These results collectively demonstrate that HI decreases the probability of misfolded pathways and enhances the preference for type I and type II pathways compared to free-draining simulations.

Here, we characterize microscopic features of type I and type II folding pathways. Figure 3(a) shows the number of native N_c [red line in Fig. 3(a)] and non-native N_n [blue line in Fig. 3(a)] hydrophobic contacts (we use cutoff distance 3σ) in the simulation $f1$ [Fig. 2(a)] with type I folding pathway. The growth of native contacts progresses stepwise. Analyzing the formation of correctly folded helices

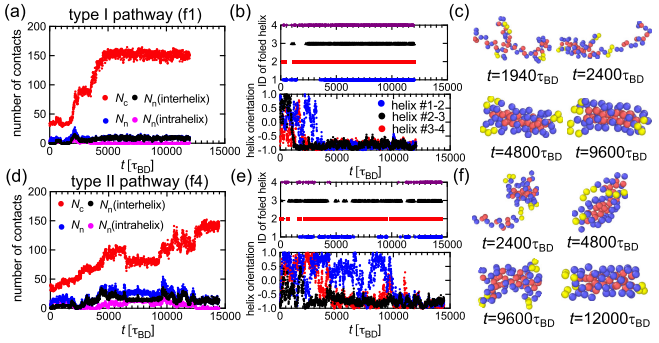

FIG. 3. Characterization of type I and type II folding pathways. We show the results for the folded trajectories $f1$ [Fig. 2(a); type I folding pathway] and $f4$ [Fig. 2(b); type II folding pathway]. (a) Temporal change of the number of native N_c (red line), non-native N_n (blue line), interhelix non-native (black line), and intrahelix non-native (magenta line) hydrophobic contact (we use cutoff 3σ) in the trajectory $f1$. (b) Top: temporal change of correct folded helices in the trajectory $f1$. Here, we calculate the order parameter $\chi(t)$ for each of the four helices and regard a helix as folded if $\chi(t) < 0.3$. Only when helix i is folded properly ($\chi_i < 0.3$), do we indicate a point on the axis of IDi. To avoid the overlap between different lines, folded helices with ID 1–4 are labeled as 1–4, respectively. Bottom: temporal change of the relative orientation between helix pair 1-2, pair 2-3, and pair 3-4 in the trajectory $f1$. Note that, in the native state, the neighboring helices are almost antiparallel. (c) Simulation snapshots of protein folding at various times in the trajectory $f1$. (d)–(f) The same characterization of the trajectory $f4$.

[Fig. 3(b), top] and the orientation of neighboring helices [Fig. 3(b), bottom] reveals that folding begins with the middle region of helices 2 and 3 arranged in an antiparallel structure [$t = 1940\tau_{BD}$ in Fig. 3(c)], followed by the addition of helix 4 [$t = 2400\tau_{BD}$ in Fig. 3(c)]. At this stage, helix 1 is still floating outside, and finally, the insertion of helix 1 occurs [$t = 4800\tau_{BD}$ in Fig. 3(c)]. This step-by-step folding process leads to minimal non-native hydrophobic contacts [blue line in Fig. 3(a)] and results in almost simultaneous folding and collapse at $t \approx 5000\tau_{BD}$ [Fig. 2(a)].

In Figs. 3(d)–3(f), we present the same analysis for the simulation $f4$ [Fig. 2(b)] with type II folding pathway. Here, we observe a higher amount of non-native hydrophobic contacts, peaking at around 40 to 50 at $t \approx 5000\tau_{BD}$ during protein collapse [Fig. 3(d)]. Unlike the type I pathway, where folding and collapsing happen nearly simultaneously, in the type II pathway, collapse ($t \approx 5000\tau_{BD}$) precedes correct folding ($t \approx 15\,000\tau_{BD}$). A detailed analysis of the collapsed structure at $t \approx 5000\tau_{BD}$ reveals the improper formation of helix 4 and incorrect relative orientation between helices 1 and 2, confirming the misfolding of the collapsed globule. This globule has a larger number of non-native hydrophobic contacts, particularly those resulting from interhelix contacts [black line in Fig. 3(d)], compared to the type I folding pathway. Thus, the protein undergoes structural relaxation until helices 1 and 2 are properly arranged into antiparallel structures [Fig. 3(e), bottom]. Typically, the type II pathway requires a slightly longer time than the type I pathway.

We also analyze misfolded pathways [Fig. 2(c)] and reveal their physical origin (Fig. 6). These misfolded pathways share a common feature: a large number of non-native hydrophobic contacts in the collapsed globule. These non-native contacts frustrate structural relaxation toward the native conformation, leading to slow folding dynamics. To demonstrate this, we choose two misfolded trajectories labeled $u1$ and $u2$ in Fig. 2(c). The temporal change in the number of native and non-native contacts [Fig. 6(a)] and correct folded helices [Fig. 6(b)] in the misfolded trajectory $u1$ reveals that the folding kinetics is accompanied by a large number of non-native contacts reaching around 60 to 70 at $t \approx 6000\tau_{BD}$ when the protein is collapsed. Even in the late stage, only helix 2 is properly folded, while the other helices remain incorrectly folded [Fig. 6(b)]. As seen in Fig. 6(c), the final collapsed state at $t = 12\,000\tau_{BD}$ significantly differs from the native conformation, suggesting a long relaxation time for folding into the native state beyond the accessible timescale of our FPD simulations. We also quantify the folding pathways of the misfolded trajectory $u2$ [Fig. 2(c)], with results shown in Figs. 6(d)–6(f). Again, many non-native contacts exist [blue line in Fig. 6(d)]. Notably, the final collapsed state at $t = 15\,000\tau_{BD}$ appears similar to the native state [Fig. 6(f)] with all four helices properly folded [Fig. 6(e), top]. However, their relative orientation is incorrect [Fig. 6(e), bottom]. For instance, in the native configuration, helices of 2–3 and 3–4 should be in an almost antiparallel arrangement; however, this is not the case in the final state [red line and black line in Fig. 6(e), bottom]. We also analyzed trajectory $u4$, revealing different misfolded structures at the microscopic level but with numerous non-native contacts (Fig. S2 in [50]). Therefore, the accumulation of many non-native hydrophobic contacts upon the collapsing is the origin of misfolded pathways with slow folding dynamics.

What, then, is the mechanism of the observed impact of HI on protein folding? Earlier works [12] have noted that the initial extended amino acid random coil resembles a swollen polymer. For the latter, it has been shown that the directional flow along the backbone accelerates collapsing [25,26,32–34,52]. We indeed find that protein collapsing [Fig. 4(a)] and early-stage native tertiary contact growth [the inset of Fig. 4(a)] occur faster with HI, supporting previous arguments [12]. However, the acceleration of collapsing alone [12,25,26,32] may not fully explain the significant difference caused by HI (Figs. 1 and 2). Particularly, considering that folding typically occurs later than collapsing, the roles of HI in protein folding should go beyond the directional flow scenario [12].

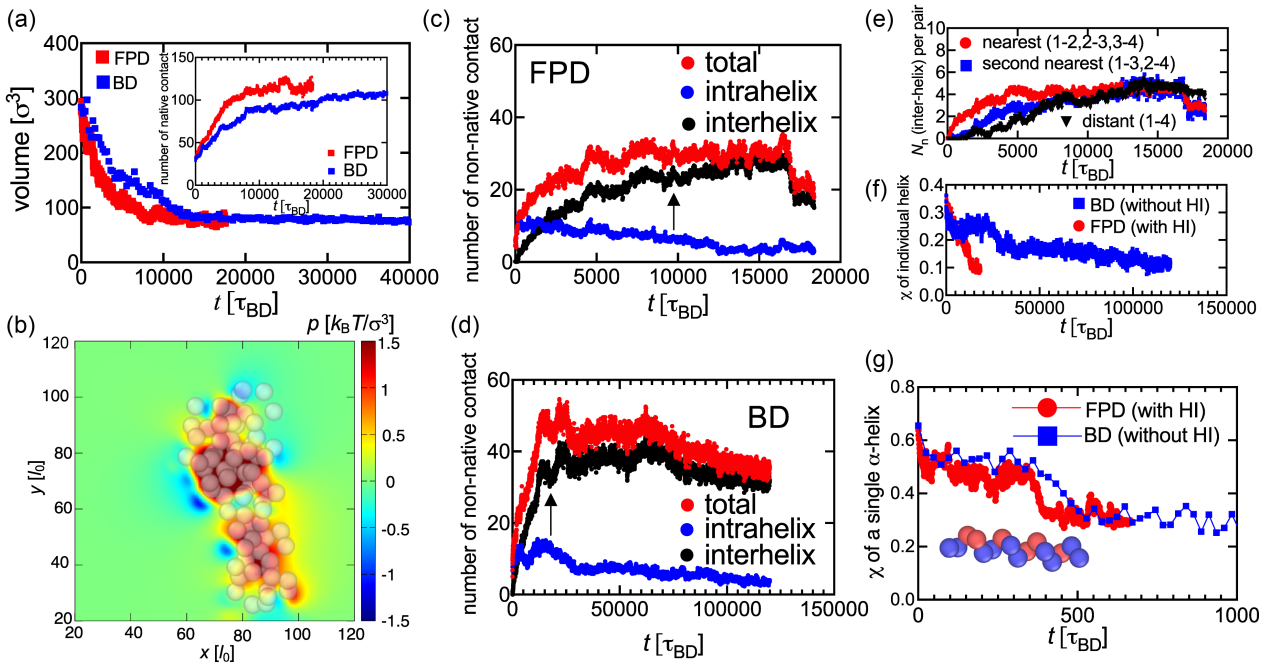

FIG. 4. Roles of hydrodynamics in protein folding. (a) Temporal change of ensemble-averaged protein volume in BD and FPD simulations. The inset shows the growing native hydrophobic contact. (b) The local pressure P of the solvent upon volume shrinking of protein. The solvent is squeezed out from the protein domain to the surroundings to satisfy the incompressibility condition $\nabla \cdot \boldsymbol{v} = 0$. Temporal evolution of ensemble-averaged non-native hydrophobic contact along with the interhelix and intrahelix parts in (c) FPD and (d) BD simulations. The arrows indicate the typical collapsing time determined from (a). (e) Temporal change of interhelix non-native hydrophobic contact between nearest (1–2, 2–3, and 3–4), second-nearest (1–3 and 2–4), and distant (1–4) neighboring helices. (f) Temporal change of order parameter χ of individual α helix in BD and FPD simulations. (g) Folding kinetics of an isolated α helix. Temporal change of order parameter χ for a single α helix in FPD and BD simulations. We utilize an initial configuration under $k_B T_{\text{init}}/\varepsilon = 1$. The inset shows the native state of a single α helix.

In our previous study of polymer collapsing, we uncovered the dual effects of HI: while it accelerates the collapsing of swollen polymers, it can also decelerate the collapsing of compact polymers due to a slow squeezing process of the solvent [33]. We speculated that this squeezing flow effect upon volume shrinking might be crucial in avoiding the establishment of non-native hydrophobic contact [11]. Indeed, we can see in Fig. 4(b) that pressure counteracts solvent flow, maintaining the incompressible condition $\nabla \cdot \boldsymbol{v} = 0$ and preventing amino acids from moving in such a way as to aggregate in one place. By comparing the ensemble-averaged number of non-native contact N_n in FPD [Fig. 4(c)] and BD [Fig. 4(d)] simulations, we can see that the squeezing flow effects of HI indeed significantly reduce the formation of such disfavored contacts by a factor of around 1.5–2 upon collapsing [as indicated by the arrows in Figs. 4(c) and 4(d)]. This indicates that HI makes the collapsed globule much closer to the native conformation and the kinetic barrier toward the native conformation significantly lower, which is critical to selecting type I and type II folding pathways. Here, we stress the importance of avoiding non-native contacts as, during protein collapse, hydrophobic beads are more prone to encountering non-native neighbors than their native counterparts. This propensity arises from the abundance of potential non-native neighbors, a quantity that scales with the number of hydrophobic beads under thermal fluctuations. Therefore, the squeezing flow does not directly facilitate the formation of native contacts; instead, it accomplishes this indirectly by preventing the buildup of non-native contacts during protein collapse. Conversely, in BD simulations, hydrophobic beads make direct contact easily without the associated squeezing flow, resulting in a higher probability of forming a random globule. This squeezing flow [Fig. 4(b)] arises only when the short-range part of HI is incorporated [33,48], a critical role overlooked in previous simulations.

Furthermore, we find that non-native hydrophobic contacts mainly occur between helices, while intrahelix contacts decrease over time [Figs. 4(c) and 4(d)]. The accumulation of interhelix non-native contacts increases in the order of nearest, second-nearest, and distant helix pairs, but each becomes almost equal in the late folding stage [Fig. 4(e)]. A large amount of interhelix non-native

contacts in BD simulations significantly slows down the folding kinetics of individual α helix [Fig. 4(f)]. As a comparison, we also simulate the folding kinetics of a single α helix [Fig. 4(g)]. We find the presence of HI slightly accelerates the folding kinetics [Fig. 4(g)], whose equilibration time is much shorter compared to that of the protein folding [Fig. 4(f)]. The acceleration in the folding kinetics of a single α helix by HI [Fig. 4(g)] is relatively weak, consistent with the minor effects reported in previous studies [26,28]. This indicates that interhelix hydrophobic miscontacts are crucial in frustrating the folding of α helices. Thus, HI exerts a more substantial influence on protein folding kinetics than on its isolated structural units. We also discuss the temperature dependence of folding kinetics in Appendix B. Additionally, we examine the folding of the β-barrel protein [13] and confirm the general applicability of the role of HI (Fig. S3 and Fig. S4 in [50]).

To summarize, we have elucidated the vital roles of HI in the folding kinetics of four-α-helices bundle protein [17] and β-barrel protein [13] using the FPD method [33,48,49]. We demonstrate that HI helps select fast folding pathways and significantly accelerates folding compared to its absence. We attribute the roles of HI to the following essential effects. First, directional flow along the polymer backbone accelerates initial collapsing, consistent with previous simulations [12,29,30]. Second, incompressibility-induced squeezing flow hinders the accumulation of non-native hydrophobic contacts, particularly in interhelix regions, preventing kinetic trapping and allowing more time for the protein to find its global minimum state. The squeezing flow is crucial throughout the folding process, an aspect often overlooked in earlier simulations. We also find that the impact of HI varies with temperature, being most pronounced under biologically relevant conditions. These findings provide fresh insights into the contributions of HI to protein folding.

We thank Michio Tateno for his technical help. This work was partially supported by the Grant-in-Aid for Specially Promoted Research (JSPS KAKENHI Grant No. JP20H05619) from the Japan Society for the Promotion of Science (JSPS). J. Y acknowledges the Recommendation Program for Young Researchers and Woman Researchers offered by Information Technology Center, the University of Tokyo and the support from Shanghai Jiao Tong University via the scholarship for outstanding Ph.D. graduates. J. Y. also thanks Prof. Changbong Hyeon (Korea Institute for Advanced Study) for insightful discussions.

Appendix A: Fluid particle dynamics simulation.—The fluid particle dynamics (FPD) method [33,48,49] resolves both the near-field and far-field HI based on the direct computation of the Navier–Stokes (NS) equation. Given that the beads in coarse-grained protein models represent entire amino acid residues that surpass water molecules in both size and mass by several multiples, they are commonly regarded as rigid objects while the solvent is treated as a continuous medium [12,17,24], allowing the use of the NS equation for describing hydrodynamic interaction (HI) [53]. In the framework of FPD, each bead is represented as a viscous fluid particle expressed by $\psi_n(\boldsymbol{r}) = \frac{1}{2}\{\tanh[(a - |\boldsymbol{r} - \boldsymbol{R}_n|)/\xi] + 1\}$, where a is the particle radius, ξ is its interface thickness, and $\boldsymbol{R}_n$ is the position vector of particle n. The flow field $\boldsymbol{v}$ is calculated by solving the NS equation $\rho[(\partial/\partial t) + \boldsymbol{v}\cdot\nabla]\boldsymbol{v} = \boldsymbol{f} + \nabla\cdot(\boldsymbol{\sigma} + \boldsymbol{\sigma}^{\mathrm{R}})$, where ρ is the constant fluid density, $\boldsymbol{f} = \sum_n \boldsymbol{F}_n\psi_n(\boldsymbol{r})/\int\psi_n(\boldsymbol{r}')d\boldsymbol{r}'$ is the smooth force field, and $\boldsymbol{F}_n = -\partial(V_{\mathrm{LJ}} + V_{\mathrm{bond}} + V_{\mathrm{angle}} + V_{\mathrm{dihedral}})/\partial\boldsymbol{R}_n$ is the body force acting on bead n. $\boldsymbol{\sigma} = \eta(\boldsymbol{r})\left(\nabla\boldsymbol{v} + (\nabla\boldsymbol{v})^{\mathsf{T}}\right) - p\boldsymbol{I}$ is the internal stress of the fluid, where $\eta(\boldsymbol{r}) = \eta_{\mathrm{s}} + (\eta_{\mathrm{p}} - \eta_{\mathrm{s}})\sum_{n=1}^{N}\psi_n(\boldsymbol{r})$ is the viscosity field, η_{s} and η_{p} are the viscosities of fluid and beads, $\boldsymbol{I}$ is the unit tensor, and p is the pressure determined to satisfy the incompressible condition $\nabla\cdot\boldsymbol{v} = 0$. We solve the NS equation by the marker-and-cell method with a staggered lattice under periodic boundary conditions [54]. The protein configuration is updated off-lattice by integrating the equation $d\boldsymbol{R}_n(t)/dt = \boldsymbol{V}_n(t)$, where $\boldsymbol{V}_n(t) = \int d^3\boldsymbol{r}(\boldsymbol{v}\psi_n(\boldsymbol{r}))$ is the particle velocity. To properly incorporate thermal fluctuations, we introduce the random fluctuating stress field $\boldsymbol{\sigma}^R$ that satisfies the fluctuation-dissipation relation $\langle\boldsymbol{\sigma}^{\mathrm{R}}\rangle = \boldsymbol{0}$ and $\langle\sigma^{\mathrm{R}}_{ij}(\boldsymbol{r},t)\sigma^{\mathrm{R}}_{kl}(\boldsymbol{r}',t')\rangle = 2\eta(\boldsymbol{r})k_{\mathrm{B}}T(\delta_{ik}\delta_{jl} + \delta_{il}\delta_{jk})\delta(t - t')$ [49,55], where δ is the Dirac delta function.

We set the length unit as lattice size l_0, the time unit as $\tau_0 = \rho l_0^2/\eta_{\mathrm{s}}$, $a = 3.2l_0$, $\xi = l_0$, $\sigma = 2a + \xi = 7.4l_0$, box size $L = 256l_0 = 34.59\sigma$, $\eta_{\mathrm{p}} = 2\eta_{\mathrm{s}}$, and time step $\Delta t = 0.025\tau_0$. We set $\beta = 1/(k_{\mathrm{B}}T) = 0.07\rho/(l_0\eta_{\mathrm{s}}^2)$ such that diffusive dynamics is achieved within a reasonable

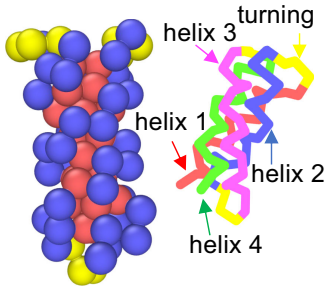

FIG. 5. The native conformation of four-α-helices bundle protein. The amino acid residues contain hydrophobic (red beads), hydrophilic (blue beads), and neutral ones (yellow beads). The linking section between the four α helices is known as the turning region.

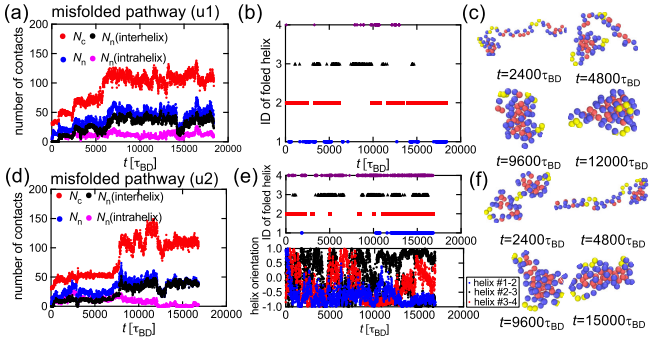

FIG. 6. Characterization of misfolded pathways. We show the results for misfolded trajectories $u1$ and $u2$ [Fig. 2(c)]. (a) Temporal change of the number of native N_c (red line), non-native N_n (blue line), interhelix non-native (black line), and intrahelix non-native (magenta line) hydrophobic contacts (we use the cutoff distance of 3σ) in trajectory $u1$. (b) Temporal change of correct folded helices in trajectory $u1$, with only helix 2 folded correctly in the late stage. (c) Simulation snapshots of protein folding at various times in trajectory $u1$. (d)–(f) Similar characterization of trajectory $u2$ [Fig. 2(c)]. In the bottom panel of (e), we show the temporal change in the relative orientation between two helices. While the α helices form in the late stage [(e), top], the relative orientation between helices 2–3 and 3–4 is incorrect.

simulation time [44]. The quench depth k_BT/ε is controlled by changing the energy coupling ε while k_BT is fixed. The simulation time is scaled by the Brownian time of a single particle $\tau_{BD} = \sigma_H^2/24D$, where D is the diffusion constant of a single particle, $\sigma_H = 8.14l_0$ is the hydrodynamic diameter, and $\lambda = \int \psi(\boldsymbol{r})d\boldsymbol{r}/\int \psi(\boldsymbol{r})^2 d\boldsymbol{r}$ is a correction factor ($\lambda \approx 1.69$ for $\xi/a = 1/3.2$) [49]. This parameter setting yields $\tau_0/\tau_{BD} \approx 0.04$. We perform multiple simulations starting with different configurations and random seeds.

We remark that incorporating the short-range part of hydrodynamics into simulations poses a challenge [39–41]. To validate our FPD method's capability in capturing this short-range HI, we calculate the viscous drag coefficient of two approaching particles with $\eta_p = 50\eta_s$. The results show a rapid increase at close distances, aligning well with the theoretical result [56] [Fig. S5(a) in [50]]. Nonetheless, a slight discrepancy arises when employing $\eta_p = 2\eta_s$. In this study, we employ $\eta_p = 2\eta_s$ to accelerate simulations by allowing the use of a larger time step while maintaining the slowing down feature upon particle contact. Notably, in our previous work [33], we observed polymer collapse deceleration induced by squeezing flow even with $\eta_p = \eta_s$. Crucially, we emphasize the significance of anticipating water permeation into beads in actual polymers and proteins. Anticipating water permeation into beads justifies selecting a smaller viscosity ratio η_p/η_s. Our findings remain consistent with $\eta_p = 50\eta_s$ (Fig. S6 in [50]).

Finally, we emphasize the significance of squeezing flow effects [33,38], also known as lubrication effects [39–43], in many-body systems. To illustrate, we examine the aggregation kinetics of 13 particles initially positioned on the 12 vertices and the center of an icosahedron [Figs. S5(b),(c) in [50]]. As these particles aggregate and form clusters, squeezing effects impede direct particle contact [Fig. S5(b) in [50]] and induce flow with transverse character due to the incompressible nature of the fluid [38]. Remarkably, squeezing flow facilitates the formation of long-lasting elongated structures [Fig. S5(c) in [50]]. However, in free-draining simulations as well as RP-tensor-based simulations, particles rapidly assemble into a densely packed cluster while maintaining symmetry during aggregation [Fig. S5(c) in [50]]. This underscores the pivotal role of squeezing flow in selecting distinct kinetic pathways. Furthermore, it implies that RP tensors [26,28–31] are inadequate in capturing the squeezing flow effects [Fig. S5(c) in [50]] [33,38]. This is due to their poor depiction of rapidly increased viscous drag as two particles are brought closer [Fig. S5(a) in [50]], highlighting the necessity of incorporating lubrication corrections [39–42].

Appendix B: Temperature dependence of protein folding.—In the main text, we focused on quench depth $k_BT/\varepsilon = 0.6$. However, it is worth noting that HI effects are also significant at $k_BT/\varepsilon = 0.65$, where HI accelerates the folding process, with nearly 50% of trajectories exhibiting rapid folding within $t \approx 1.5 \times 10^4 \tau_{BD}$ (Fig. 7). This observation is qualitatively similar to the findings for $k_BT/\varepsilon = 0.6$. Increasing the temperature from $k_BT/\varepsilon = 0.6$ to $k_BT/\varepsilon = 0.65$ enhances the probability of successful folding due to the increased thermal fluctuations, promoting faster structural relaxation of the collapsed globule toward the native conformation. Nevertheless, HI consistently leads to faster folding, particularly through selecting type I folding pathways (Fig. 7).

The range of quench depths that we have examined, $k_BT/\varepsilon = 0.6$–0.65, corresponds to scaled temperatures $T/T_f = 0.86$–0.93, where $k_BT_f/\varepsilon \simeq 0.7$ is the folding temperature. Assuming a physiological temperature of $T \simeq 309$ K, this yields folding temperatures of $T_f = 343$–360 K(70–86 °C) and an energy scale of $\varepsilon \approx 1$ Kcal$/N_A$, where N_A is the Avogadro constant. These values fall within reasonable parameters for many proteins. Therefore, we expect that the range of $k_BT/\varepsilon = 0.6$–0.65, where the impact of HI is significant, is critical to biological cells. Conversely, when the temperature is either much lower than or too close to the folding temperature, folding dynamics can be slowed down [Fig. S7 in [50]] by either kinetic trapping or strong thermal fluctuations [28,57],

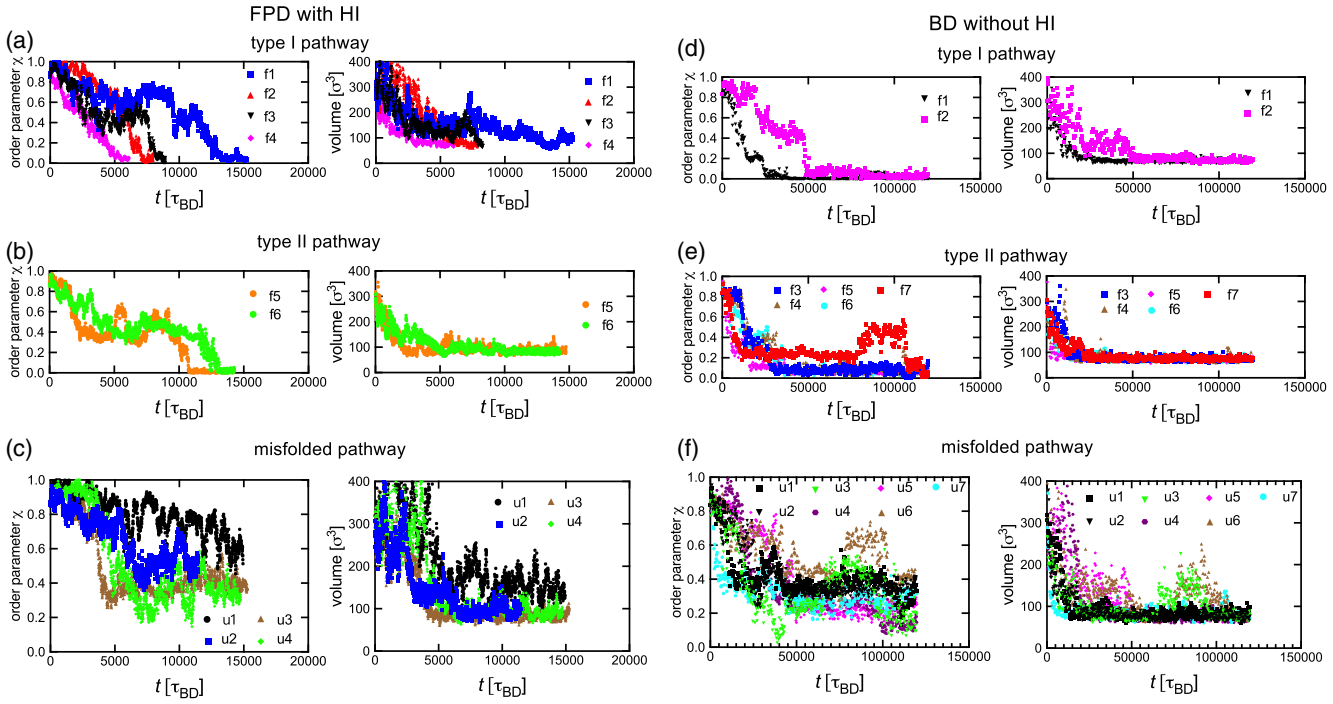

FIG. 7. Folding kinetics of four-α-helices bundle protein at the temperature $k_B T/\varepsilon = 0.65$. Temporal change of the order parameter χ and protein volume for type I, type II, and misfolded pathways in (a)–(c) FPD and (d)–(f) BD simulations. The protein volume is determined by calculating the convex hull [51] of amino acid residues.

resulting in weaker impacts of HI [Fig. S8 in [50]]. However, such extreme conditions are rarely encountered in protein folding in living cells. This suggests that proteins are designed to maximize their folding capability under physiological conditions.

*Corresponding author: tanaka@iis.u-tokyo.ac.jp

[1] Arthur Lesk, *Introduction to Protein Science: Architecture, Function, and Genomics* (Oxford University Press, Oxford, U.K., 2010).
[2] John Jumper, Richard Evans, Alexander Pritzel, Tim Green, Michael Figurnov, Olaf Ronneberger, Kathryn Tunyasuvunakool, Russ Bates, Augustin Žídek, Anna Potapenko *et al.*, Highly accurate protein structure prediction with AlphaFold, Nature (London) **596**, 583 (2021).
[3] James P. Roney and Sergey Ovchinnikov, State-of-the-art estimation of protein model accuracy using AlphaFold, Phys. Rev. Lett. **129**, 238101 (2022).
[4] Christopher M. Dobson, Protein folding and misfolding, Nature (London) **426**, 884 (2003).
[5] D. Thirumalai, Edward P. O'Brien, Greg Morrison, and Changbong Hyeon, Theoretical perspectives on protein folding, Annu. Rev. Biophys. **39**, 159 (2010).
[6] Peter L. Freddolino, Christopher B. Harrison, Yanxin Liu, and Klaus Schulten, Challenges in protein-folding simulations, Nat. Phys. **6**, 751 (2010).
[7] Anne Gershenson and Lila M. Gierasch, Protein folding in the cell: Challenges and progress, Curr. Opin. Struct. Biol. **21**, 32 (2011).
[8] S. Walter Englander and Leland Mayne, The nature of protein folding pathways, Proc. Natl. Acad. Sci. U.S.A. **111**, 15873 (2014).
[9] Jane Clarke and Rohit V. Pappu, Editorial overview: Protein folding and binding, complexity comes of age, Curr. Opin. Struct. Biol. **42**, v (2017).
[10] Rafael Tapia-Rojo, Marc Mora, Stephanie Board, Jane Walker, Rajaa Boujemaa-Paterski, Ohad Medalia, and Sergi Garcia-Manyes, Enhanced statistical sampling reveals microscopic complexity in the talin mechanosensor folding energy landscape, Nat. Phys. **19**, 52 (2022).
[11] Hajime Tanaka, Roles of hydrodynamic interactions in structure formation of soft matter: Protein folding as an example, J. Phys. Condens. Matter **17**, S2795 (2005).
[12] Piotr Szymczak and Marek Cieplak, Hydrodynamic effects in proteins, J. Phys. Condens. Matter **23**, 033102 (2010).
[13] J. D. Honeycutt and D. Thirumalai, Metastability of the folded states of globular proteins, Proc. Natl. Acad. Sci. U.S.A. **87**, 3526 (1990).
[14] J. D. Honeycutt and D. Thirumalai, The nature of folded states of globular proteins, Biopolymers **32**, 695 (1992).
[15] Nicholas D. Socci and José Nelson Onuchic, Kinetic and thermodynamic analysis of proteinlike heteropolymers: Monte Carlo histogram technique, J. Chem. Phys. **103**, 4732 (1995).
[16] Z. Guo and D. Thirumalai, Kinetics of protein folding: Nucleation mechanism, time scales, and pathways, Biopolymers **36**, 83 (1995).
[17] Z. Guo and D. Thirumalai, Kinetics and thermodynamics of folding of a *de Novo* designed four-helix bundle protein, J. Mol. Biol. **263**, 323 (1996).

[18] Z. Guo and D. Thirumalai, The nucleation-collapse mechanism in protein folding: Evidence for the non-uniqueness of the folding nucleus, Folding Des. **2**, 377 (1997).
[19] Vijay S. Pande and Daniel S. Rokhsar, Molecular dynamics simulations of unfolding and refolding of a β-hairpin fragment of protein G, Proc. Natl. Acad. Sci. U.S.A. **96**, 9062 (1999).
[20] D. K. Klimov and D. Thirumalai, Mechanisms and kinetics of β-hairpin formation, Proc. Natl. Acad. Sci. U.S.A. **97**, 2544 (2000).
[21] Scott Brown, Nicolas J. Fawzi, and Teresa Head-Gordon, Coarse-grained sequences for protein folding and design, Proc. Natl. Acad. Sci. U.S.A. **100**, 10712 (2003).
[22] Troy Cellmer, Dusan Bratko, John M. Prausnitz, and Harvey Blanch, The competition between protein folding and aggregation: Off-lattice minimalist model studies, Biotechnol. Bioeng. **89**, 78 (2005).
[23] Tristan Bereau and Markus Deserno, Generic coarse-grained model for protein folding and aggregation, J. Chem. Phys. **130**, 235106 (2009).
[24] Changbong Hyeon and D. Thirumalai, Capturing the essence of folding and functions of biomolecules using coarse-grained models, Nat. Commun. **2**, 487 (2011).
[25] Rakwoo Chang and Arun Yethiraj, Solvent effects on the collapse dynamics of polymers, J. Chem. Phys. **114**, 7688 (2001).
[26] N. Kikuchi, J. F. Ryder, C. M. Pooley, and J. M. Yeomans, Kinetics of the polymer collapse transition: The role of hydrodynamics, Phys. Rev. E **71**, 061804 (2005).
[27] Jiaxing Yuan and Hajime Tanaka, Hydrodynamic effects on the collapse kinetics of flexible polyelectrolytes, Phys. Rev. Lett. **132**, 038101 (2024).
[28] A. Baumketner and Y. Hiwatari, Influence of the hydrodynamic interaction on kinetics and thermodynamics of minimal protein models, J. Phys. Soc. Japan **71**, 3069 (2002).
[29] Marek Cieplak and Szymon Niewieczerzał, Hydrodynamic interactions in protein folding, J. Chem. Phys. **130**, 124906 (2009).
[30] Tamara Frembgen-Kesner and Adrian H. Elcock, Striking effects of hydrodynamic interactions on the simulated diffusion and folding of proteins, J. Chem. Theory Comput. **5**, 242 (2009).
[31] Fabio C. Zegarra, Dirar Homouz, Yossi Eliaz, Andrei G. Gasic, and Margaret S. Cheung, Impact of hydrodynamic interactions on protein folding rates depends on temperature, Phys. Rev. E **97**, 032402 (2018).
[32] Tri Thanh Pham, Mohit Bajaj, and J. Ravi Prakash, Brownian dynamics simulation of polymer collapse in a poor solvent: Influence of implicit hydrodynamic interactions, Soft Matter **4**, 1196 (2008).
[33] Kumiko Kamata, Takeaki Araki, and Hajime Tanaka, Hydrodynamic selection of the kinetic pathway of a polymer coil-globule transition, Phys. Rev. Lett. **102**, 108303 (2009).
[34] Tri Thanh Pham, Burkhard Dünweg, and J. Ravi Prakash, Collapse dynamics of copolymers in a poor solvent: Influence of hydrodynamic interactions and chain sequence, Macromolecules **43**, 10084 (2010).
[35] Jens Rotne and Stephen Prager, Variational treatment of hydrodynamic interaction in polymers, J. Chem. Phys. **50**, 4831 (1969).
[36] Donald L. Ermak and J. Andrew McCammon, Brownian dynamics with hydrodynamic interactions, J. Chem. Phys. **69**, 1352 (1978).
[37] Hajime Tanaka and Takeaki Araki, Viscoelastic phase separation in soft matter: Numerical-simulation study on its physical mechanism, Chem. Eng. Sci. **61**, 2108 (2006).
[38] Akira Furukawa and Hajime Tanaka, Key role of hydrodynamic interactions in colloidal gelation, Phys. Rev. Lett. **104**, 245702 (2010).
[39] Louis Durlofsky, John F. Brady, and Georges Bossis, Dynamic simulation of hydrodynamically interacting particles, J. Fluid Mech. **180**, 21 (1987).
[40] N.-Q. Nguyen and A. J. C. Ladd, Lubrication corrections for lattice-Boltzmann simulations of particle suspensions, Phys. Rev. E **66**, 046708 (2002).
[41] John F. Brady and Georges Bossis, Stokesian dynamics, Annu. Rev. Fluid Mech. **20**, 111 (1988).
[42] B. Cichocki, M. L. Ekiel-Jeżewska, and E. Wajnryb, Lubrication corrections for three-particle contribution to short-time self-diffusion coefficients in colloidal dispersions, J. Chem. Phys. **111**, 3265 (1999).
[43] Sangtae Kim and Seppo J. Karrila, *Microhydrodynamics: Principles and Selected Applications* (Courier Corporation, Massachusetts, US, 2013).
[44] Michio Tateno and Hajime Tanaka, Numerical prediction of colloidal phase separation by direct computation of Navier–Stokes equation, npj Comput. Mater. **5**, 40 (2019).
[45] Michio Tateno and Hajime Tanaka, Power-law coarsening in network-forming phase separation governed by mechanical relaxation, Nat. Commun. **12**, 912 (2021).
[46] Stany Gallier, François Peters, and Laurent Lobry, Simulations of sheared dense noncolloidal suspensions: Evaluation of the role of long-range hydrodynamics, Phys. Rev. Fluids **3**, 042301(R) (2018).
[47] Jiaxing Yuan, Kyohei Takae, and Hajime Tanaka, Impact of inverse squeezing flow on the self-assembly of oppositely charged colloidal particles under electric field, Phys. Rev. Lett. **129**, 248001 (2022).
[48] Hajime Tanaka and Takeaki Araki, Simulation method of colloidal suspensions with hydrodynamic interactions: Fluid particle dynamics, Phys. Rev. Lett. **85**, 1338 (2000).
[49] Akira Furukawa, Michio Tateno, and Hajime Tanaka, Physical foundation of the fluid particle dynamics method for colloid dynamics simulation, Soft Matter **14**, 3738 (2018).
[50] See Supplemental Material at http://link.aps.org/supplemental/10.1103/PhysRevLett.132.138402 for information about simulation details, analysis methods, and additional characterization of protein folding kinetics.
[51] C. Bradford Barber, David P. Dobkin, and Hannu Huhdanpaa, The quickhull algorithm for convex hulls, ACM Trans. Math. Softw. **22**, 469 (1996).
[52] N. Kikuchi, A. Gent, and J. M. Yeomans, Polymer collapse in the presence of hydrodynamic interactions, Eur. Phys. J. E **9**, 63 (2002).
[53] Nikita Kavokine, Roland R. Netz, and Lydéric Bocquet, Fluids at the nanoscale: From continuum to subcontinuum transport, Annu. Rev. Fluid Mech. **53**, 377 (2021).

[54] Francis H. Harlow and J. Eddie Welch, Numerical calculation of time-dependent viscous incompressible flow of fluid with free surface, Phys. Fluids **8**, 2182 (1965).

[55] Jose M. Ortiz De Zarate and Jan V. Sengers, *Hydrodynamic Fluctuations in Fluids and Fluid Mixtures* (Elsevier, Amsterdam, Netherlands, 2006).

[56] Benjamin D. Goddard, R. D. Mills-Williams, and Jin Sun, The singular hydrodynamic interactions between two spheres in stokes flow, Phys. Fluids **32** (2020).

[57] N. D. Socci, José N. Onuchic, and Peter G. Wolynes, Diffusive dynamics of the reaction coordinate for protein folding funnels, J. Chem. Phys. **104**, 5860 (1996).